

LA-UR-81-1734

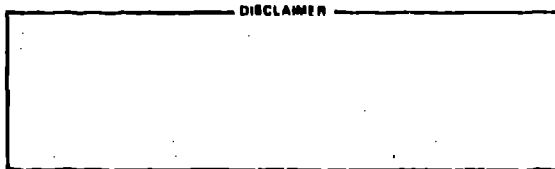
TITLE: NEW TECHNIQUES AND PHENOMENA AT MULTIMEGABAR DYNAMIC PRESSURES

AUTHOR(S): John W. Shaner

MASTER

SUBMITTED TO: Talk to be presented at the American Chemical Society "State-of-the-Art Symposium" on High Pressure in Washington, D. C., June 8-10, 1981

University of California



By acceptance of this article, the publisher recognizes that the U.S. Government retains a nonexclusive, royalty-free license to publish or reproduce the published form of this contribution, or to allow others to do so, for U.S. Government purposes.

The Los Alamos Scientific Laboratory requests that the publisher identify this article as work performed under the auspices of the U.S. Department of Energy.



LOS ALAMOS SCIENTIFIC LABORATORY

Post Office Box 1683 Los Alamos, New Mexico 87545

An Affirmative Action/Equal Opportunity Employer

DISTRIBUTION OF THIS DOCUMENT IS UNLIMITED

285

NEW TECHNIQUES AND PHENOMENA AT MULTIMEGABAR DYNAMIC PRESSURES*

J. W. Shaner
Los Alamos National Laboratory
Los Alamos, New Mexico 87545

ABSTRACT

At pressures beyond the range of contemporary diamond anvil technology, we expect a wealth of unexplored changes in the properties of materials, such as the appearance of new solid phases and large increases in melting temperatures. From a practical standpoint, multi-megabar pressures still require dynamic compressions because of the difficulty of containing a very high energy-density. Shock waves have been a convenient way of producing fairly well-defined material states at multi-megabar pressures. However, the rapid temperature rise associated with strong shocks has obscured some of the interesting material behavior. On the other hand, the temperature rise makes shock wave techniques ideal for studying melting phenomena at very high pressures.

By accurately measuring the velocity of sound in a shock compressed medium, we effectively obtain a derivative of the equation-of-state surface. In addition to this new information, the sound velocity is sensitive to changes of state. Another sensitive detector of phase changes is the temperature behind a shock front. By measuring temperatures and sound velocities we have been able to detect previously unmeasured solid-solid and melting transitions.

BACKGROUND

The use of shock waves in the investigation of material properties at very high pressures has already had a long history. Subject to the validity of a few simplifying assumptions, a shock wave produces a reasonably well defined thermodynamic state of both elevated pressure and elevated temperature, in samples which may be several cubic centimeters or larger in size. With the assumption of a steady propagating shock wave, the conservation of mass, momentum, and energy lead respectively to the three Hugoniot equations relating the state of the shock compressed material to that of the uncompressed material:

$$V = V_0 (1 - U_p/U_s) \quad (1)$$

$$\rho_1 - \rho_0 = \rho_0 U_p/U_s \quad (2)$$

$$E - E_0 = \frac{1}{2} (\rho_1 - \rho_0) (V_0 - V)^2 \quad (3)$$

In equations 1 through 3, U_s is the shock velocity, U_p is the material velocity behind the shock, V is the specific volume, ρ_1 is the stress component along the shock propagation direction, and E is the internal

energy. The measurement of U_s and U_p along with the initial conditions of the material are sufficient to describe the thermodynamic state behind the shock front. The locus of such states starting from a common initial condition is referred to as the Hugoniot curve, and it lies on, or close to the equilibrium equation of state surface.

The assumption that a strong shock propagates as a steady wave is generally consistent with measurement. Weak shock waves, where the longitudinal elastic precursors are not overdriven, generally are not steady, although portions of even these wave fronts may achieve a steady state - (1).** The phenomena described in this paper all relate to strong shock conditions, where the steady wave assumption is good.

Another assumption is that thermodynamic equilibrium is established behind the shock front. Although the time intervals are very short, experimental evidence indicates that equilibrium is very quickly established, with perhaps two notable exceptions. Some phase transitions, such as that from graphite to diamond, are notoriously sluggish. This one is seen in shock waves, but at substantially higher pressures and temperatures than is required to convert graphite to diamond statically. Also, in samples recovered after shock loading, we find evidence for a non-equilibrium concentration of defects. Most shock recovery experiments involve complex unloading and reloading processes, so any deduction concerning the state of materials behind the first shock should be taken with caution.

The problem of non-equilibrium densities has also been raised - (2). Although no direct measurement has ever been made of densities of shock compressed materials to better than a few percent - (3), we believe the densities to be close to equilibrium. In particular, by calibrating ruby fluorescence against shock experiments on copper - (4), and then comparing static and dynamic experiments on iron, one obtains agreement on the isothermal compression curve consistent with experimental uncertainties of a few percent - (5). If the defects contribute to the density, either the contribution is small, or it is virtually identical for very different metals. We feel the latter possibility is unlikely.

Another assumption deserves mention. The stress in equation (2) refers to a longitudinal component and not the pressure. The fact that non-zero stress deviators may exist behind a shock wave in a solid was recognized from the very beginning of such experiments - (6). We are only now beginning to get quantitative data concerning the relationship between the measured longitudinal stress and the mean stress or pressure. Of particular significance are the density and temperature dependence of the effective flow stress and the question of how close to a hydrostat the material behind a shock wave lies. We have accumulated data over the last two decades

* This work was performed under the auspices of the United States Department of Energy.

** Numbers in parentheses designate references at the end of the paper.

indicating that, as expected, the flow stress does increase with increasing density, at least until high temperature effects dominate - (7,8). However, recent experiments by Asay have shown that in the case of aluminum shocked to over 21 GPa the state of the material appears to be within 0.2 GPa of hydrostatic conditions - (9). We can interpret the low value of the shear stress in a shocked metal in terms of the adiabatic shear model developed by Grady - (10). In this model, the shearing occurs locally in bands, where the internal energy increases unstably. As a result, the material may have little macroscopic shear strength. Although the available experimental evidence supports these ideas, the data necessary for a complete quantitative model of the pressure dependence of stress deviators are still incomplete. With more complete data we should be able to make consistent solid strength corrections to all of our shock wave data.

One further limitation of shock waves as a means of studying materials at high pressure is a result of the particular track the Hugoniot curve makes in thermodynamic space. If the shock strength is parameterized by U_p , one can see by differentiating equations 2 and 3 that both pressure and internal energy (or entropy) increase together, except in the most pathological cases. As a result, those transitions like normal melting, where internal energy increases from the solidus to liquidus, but the transition pressure increases with the density, are indicated by only subtle changes in slope in the curve of U_p vs U_p . As an indication of the subtlety, we show in Fig. 1 the Hugoniot curve for lead in the region where melting should be taking place. The experiments give no indication of a melting transition.

The new techniques described in the next sections overcome some of the shortcomings of shock waves as a means of studying materials at high pressures. In particular, we describe three new techniques which allow one to detect new phase transitions and to measure new details of the thermal and mechanical behavior of shock compressed materials.

OPTICAL PYROMETRY

From equation 3 we see that the thermal parameter measured in a shock wave experiment is internal energy. In his early work - (11), Kormer showed that one might be able to measure the temperature as well

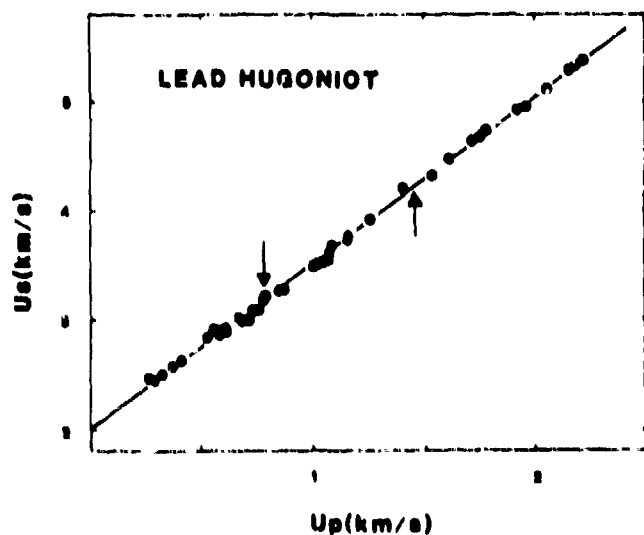


Fig. 1. Shockwave data for lead. The region where we expect melting to occur is between the arrows.

in a shock compressed transparent material by high speed optical pyrometry. In addition to providing heat capacity data, certain phase transitions showed up much more clearly in the pressure-temperature representation than in the pressure-energy plane.

This work formed the conceptual basis for two sets of pyrometric measurements on shocked SiO_2 , one set by McQueen at Los Alamos - (12) and another by Lyzenga at Cal Tech - (13). When a strong shock propagates into a transparent sample, the thermal radiation from the hot compressed material can pass through the uncompressed material and into a fast optical pyrometer. In these experiments, McQueen used a rotating mirror streaking camera with a detonation wave in nitromethane as a calibration standard. Lyzenga used silicon photodiodes and color filters calibrated against a tungsten ribbon lamp. The data from both sets of measurements are shown in Fig. 2. In order to make the comparison, average emissivities from Lyzenga's measurements were used. The agreement, within 5% in absolute temperature, is excellent for such measurements above 5000 K and with time resolution of less than 10 ns.

Several surprises appeared in this work. Firstly, even at shock temperatures below 5000 K, the rise time of the optical signal was less than 10 ns. Therefore we may say that a layer of shocked material less than 100 μm thick is opaque. We expect that a wide gap insulator like stishovite should still be optically thin under these conditions, unless there are many defect electronic states in the gap. If that is true, we worry about whether the radiation is grey body and whether the apparent temperatures represent equilibrium. Measurements by Lyzenga - (14) indicate a good fit to a grey body spectrum, so at least the radiation appears to be thermal.

The next surprise was the region for both fused silica and crystal quartz where increasing shock pressure (and internal energy) decreases the apparent temperature. This indication of a phase change cannot be detected in conventional shock measurements on SiO_2 . The anomalous behavior can be explained in two ways. The Hugoniot may follow an equilibrium phase line with negative dT/dP . The shock temperatures are such that we suspect the new phase change to be

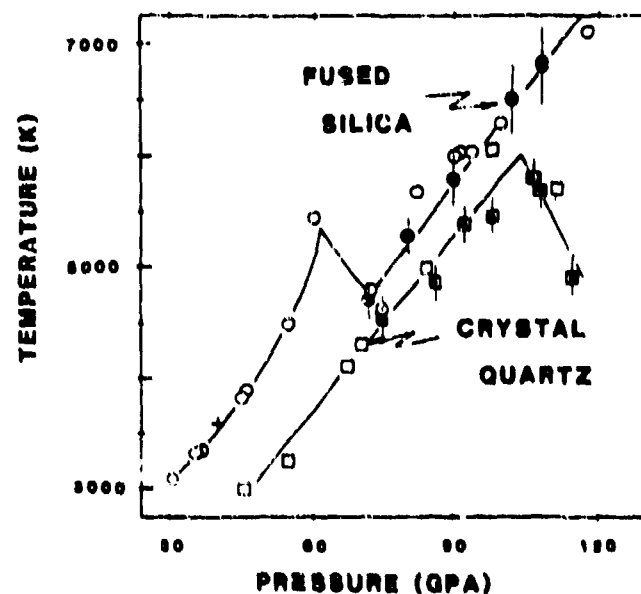


Fig. 2. Analyzed pyrometric data for shock compressed SiO_2 . Solid symbols are from Lyzenga - (13), open symbols are from McQueen - (12).

melting, in which case the silica melt is denser than the solid. On the other hand, the discrepancy in location of the phase boundary for the fused silica and the quartz suggests complex high temperature phase behavior or non-equilibrium effects. The latter explanation has been proposed by Lyzenga - (13). Both transitions are then supposed to be melting from a superheated solid. Although one rarely can superheat a solid, and certainly not by 1000 K under normal conditions, in these experiments we are looking less than 100 μm into the shocked material. At this depth, the material is only a few nanoseconds behind the onset of the shock. These experiments may in fact be the first observation of a limit on the time scale necessary for a melting transition.

In order to resolve the uncertainty in the interpretation of the SiO_2 results we must pursue both more carefully controlled shock waves with faster pyrometry, and similar experiments around better known phase transitions. Examples of the latter would be the melting transitions in the alkali halides. On the other hand, optical pyrometry has already proven to be a viable technique, as well as a means to observe high pressure phase behavior which is not accessible by any other means.

THE OPTICAL ANALYZER

We have seen that the radiation from shocked transparent materials may be thermal and that the optical depth may be very small. These ideas lead to a scheme for measuring release wave velocities in shock compressed media. The information contained in this data includes longitudinal and bulk sound velocities. The optical analyzer scheme, developed by McQueen - (15), is based on the use of a short shock illustrated in Fig. 3. If a thin flyer plate impacts a target, shocks propagate forward in the target and backward in the flyer. The interaction of the shock with the flyer free surface results in a release wave coming forward again with the velocity of sound in the compressed medium. Typically this rarefaction travels faster than the shock, which in turn is supersonic with respect to the uncompressed medium. When the rarefaction catches the shock front, the peak pressure starts to diminish. At this point two measurable physical phenomena occur. First the shock velocity decreases with the peak pressure. In the limit of zero pressure increase, the disturbance travels with the longitudinal elastic velocity in the uncompressed

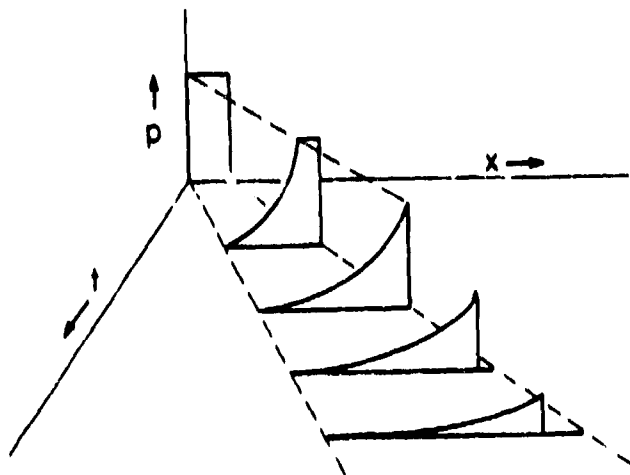


Fig. 3. Propagation of a shock of short duration. The shock front moves with constant velocity until the release catches up.

material. Secondly, the temperature drops with the peak pressure.

Since the thermal radiation varies with a high power of the temperature ($\propto T^4$ on the blue side of the black body peak) and temperature varies between the first and second power of the stress, small changes in stress make large changes in light intensity. Also, if the source is optically thick, we will see the decrease in thermal radiation within a few nanoseconds of the catch-up time.

For use with metal targets, the technique consists of propagating a short shock through varying thicknesses of target backed with a transparent radiator. For a thin target, the short shock travels a longer time in the radiator with a constant peak pressure and radiation intensity before catch-up. A thicker target will result in a shorter time of constant radiation intensity. Actual thermal radiation signals recorded by photomultipliers are shown in Fig. 4 for two different target thicknesses and three analyzer materials.

If we plot the time interval of constant thermal radiation against target thickness, we get a straight line. We have shown this to be rigorously true from similarity arguments - (15). By extrapolating down to zero time we get the target thickness required for the release to catch up at the target-analyzer interface. By this means we avoid all corrections for wave interaction at the interface. The data from Fig. 4 is plotted in Fig. 5 to show that the measurements do not depend on the analyzer material. From this target thickness and the known flyer thickness we can calculate the release wave velocity.

The kind of release wave structure we are looking for has been described previously by Aray at pressures below 10 GPa. In both porous aluminum - (16) and in bismuth - (17), he found that the leading edge of the release wave moving into solid material propagated with the longitudinal sound velocity,

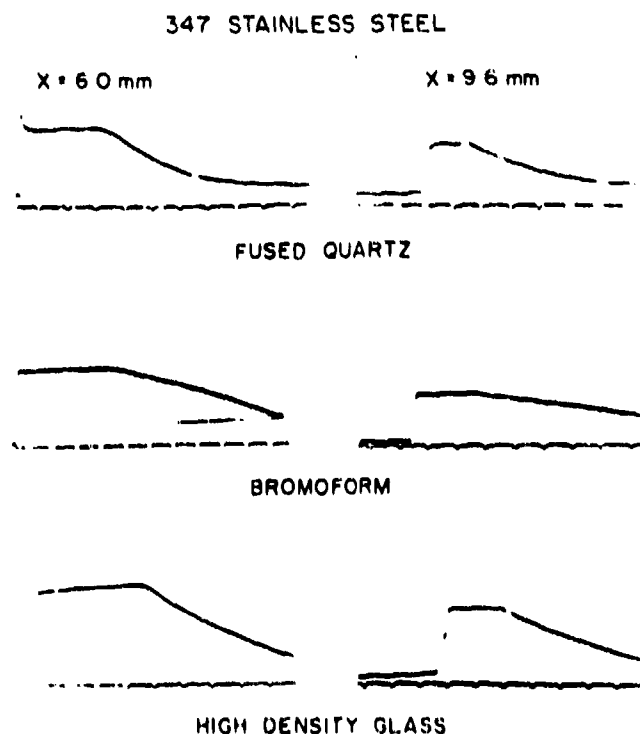


Fig. 4. Thermal radiation signals, recorded by photomultipliers, from three different optical analyzers and two target thicknesses of stainless steel. The time marks are at 100 ns intervals.

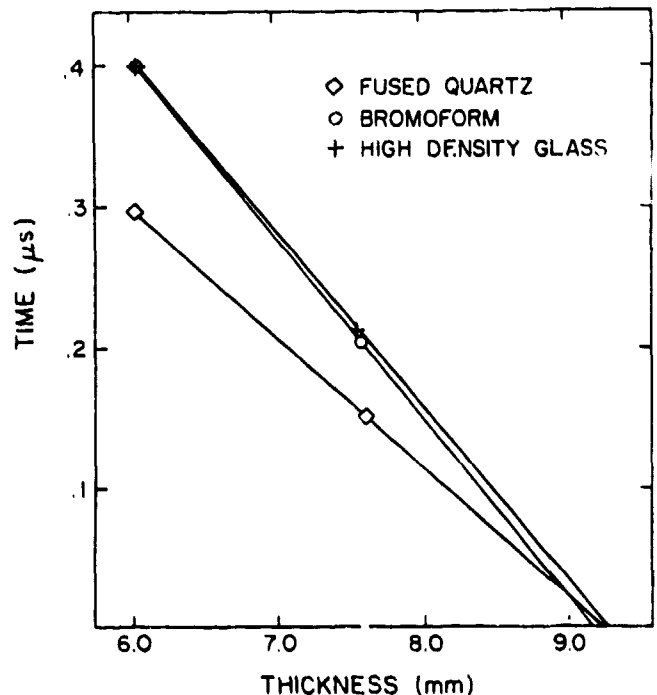


Fig. 5. Duration of constant thermal radiation intensity as a function of target thickness for the experiments shown in Fig. 4.

$C_B^2 = (B + 4\mu/3)/\rho$, where B is the bulk modulus and μ is the shear modulus. In each case when the shock was intense enough to give as little as 20% melt fraction, the leading edge of the release wave had slowed to the calculated bulk sound velocity, $C_B = B/\rho$. Both of these experiments were done at sufficiently low pressures that there was little uncertainty about the location of the melting transition. Since the optical analyzer has none of the high pressure limitations of the interface velocity interferometer used by Aray, we could extend this kind of measurement to pressures in excess of 100 GPa. At very high pressures there is considerable uncertainty in the melting points of even simple solids.

The first application of the optical analyzer has been to the melting region for iron by Brown and McQueen - (18). They measured the velocity of the beginning of the release wave in iron shocked to pressures as high as 260 GPa. Surprisingly, in experiments using thin iron flyer plates driven by both explosives and our two-stage light gas gun, they obtained consistent results showing two breaks in the release velocity as a function of shock pressure. These data are shown in Fig. 6. Since we expect no sharp changes in the thermophysical properties of fluid iron, we have interpreted the upper break as the melting of iron and the lower break as a solid-solid phase change. This interpretation is made more plausible by Fig. 7, where the iron Hugoniot is plotted in the known and extrapolated phase diagram for iron. The Hugoniot may cross the α (hcp) to γ (fcc) phase boundary before melting occurs. The upper break would then represent the γ to liquid solidus. We also show in Fig. 7, if our interpretation is correct, that melting of iron even at 260 GPa and 5500 K agrees reasonably well with a heat calculation using the Lindemann melting criterion. Use of the Kraut Kennedy criterion - (19) gives a melting curve at much lower temperatures.

These experiments show the optical analyzer technique to be a very effective means to detect high pressure phase transitions. Neither of those found in

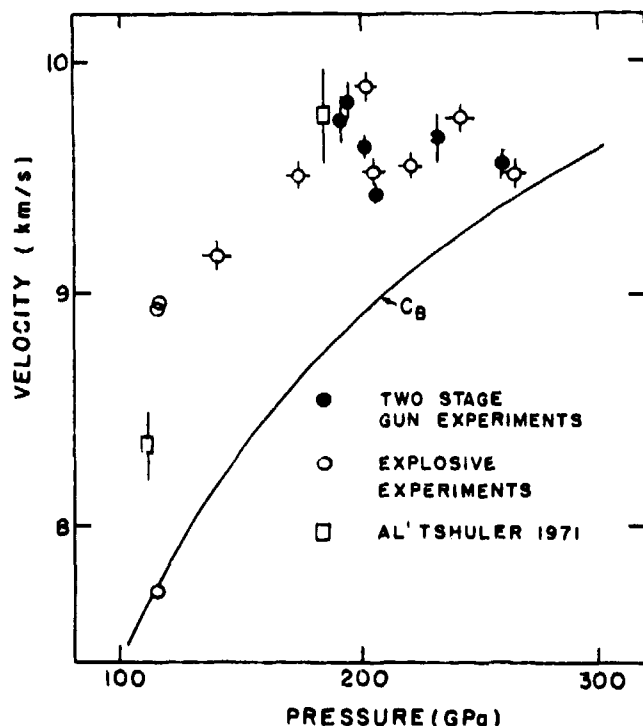


Fig. 6. Velocity of the head of the release wave as a function of initial shock pressure for iron. The highest pressure data points are on the calculated bulk wave velocity.

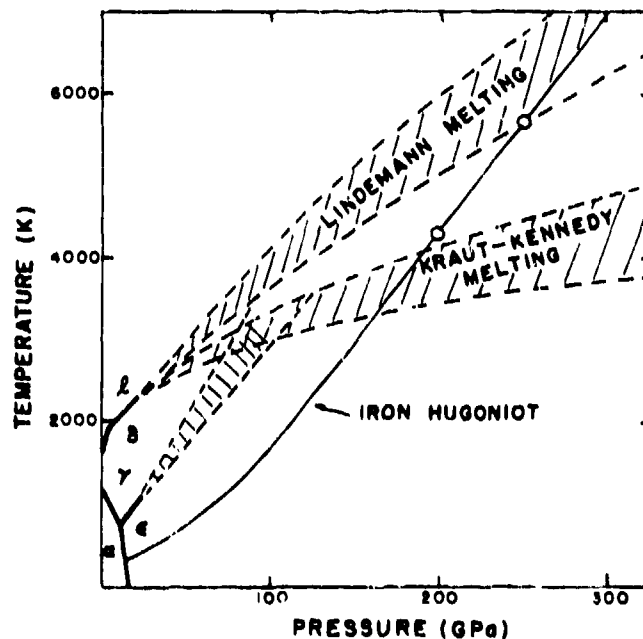


Fig. 7. Phase diagram for iron. The known region is indicated by solid lines in the lower left corner. We indicate the ranges for both Lindemann and Kraut-Kennedy melting models.

iron can be detected in the conventional shock wave measurements. The particular sensitivity of the thermal radiation makes small changes in driving stress easy to detect, and the extrapolation procedure eliminates the need for corrections to account for stress wave interactions with the interfaces. However, the extreme non-linearity of the thermal

radiation vs stress makes it very difficult to extract anything but the velocity of the head of the rarefaction wave. More quantitative results for the high pressure mechanical properties are described in the next section.

AXIALLY SYMMETRIC MAGNETIC PROBE

The axially symmetric magnetic (ASM) probe is another new technique we are exploiting in order to overcome the pressure limitations on velocity interferometry. This technique was originally developed by Fritz, et al. - (20,21). The ASM measurement consists of a static magnetic field set up by a cylindrical magnet surrounded by a coaxial loop antenna. When a metal sample is shocked and starts to move, the magnetic field distribution is deformed in such a way that voltage is induced in the pick-up loop. Thus, we measure U_p of the metal behind the shock wave.

A typical assembly for an explosive driven experiment is shown in Fig. 8. As in the interferometer measurements a non-conducting window is placed over the sample free surface to prevent uncontrolled spray coming off and confusing the measurement. The window, if matched in impedance to the metal, also minimizes confusion due to wave interaction at the interface. However, for the ASM probe there is no requirement that the window stay transparent or have a calibrated refractive index as a function of stress. The only requirement is that the resistivity stay above 10^4 - $10^5 \mu\Omega\text{-cm}$, so no flux will be trapped during the several hundred nanoseconds of the experiment. On the other hand, calibration of the system is more difficult than the interferometer, particularly if corrections for flux diffusion in the metal or trapping in the window are necessary.

We show in Fig. 9 a typical wave profile for a 2024 aluminum target backed by a teflon window, shocked to 55 GPa - (22). The time t_3 denotes the arrival of the shock at the aluminum-teflon interface. Similarly, t_8 and t_{10} denote the arrival times of the longitudinal elastic and bulk parts of the release wave at this same interface. The time t_d denotes demagnetization of the magnet when the shock wave impacts it. From the U_p measured before t_8 and the U_p measured by the time interval t_3 - t_d we can obtain the Hugoniot state in the teflon, and by standard shock impedance matching techniques we can tell the Hugoniot state of the aluminum. We can also measure the Hugoniot state in the aluminum independently, so the initial shock state is well characterized.

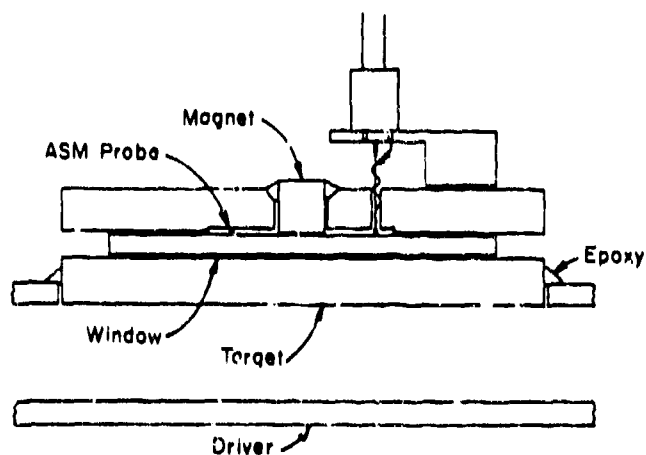
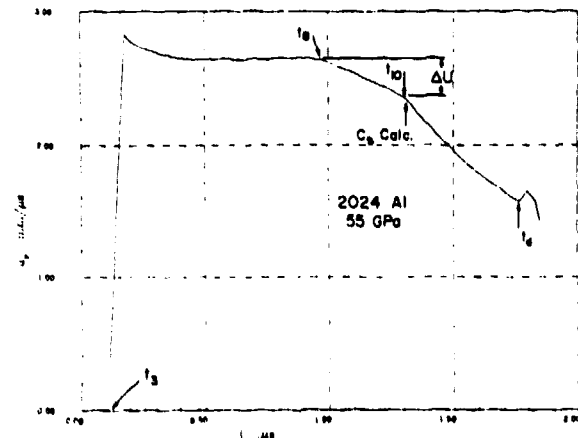


Fig. 8. Assembly for an interface velocity experiment using the ASM probe.



CEM 22 RI 8 368 2024 AL/9 009 2024 AL//10 980 TEFLON//25 497

Fig. 9. A typical analyzed material velocity record for aluminum shocked to 55 GPa, backed by a teflon window.

We show in Fig. 10 some preliminary ASM probe data on the change of longitudinal elastic wave velocity in aluminum as a function of Hugoniot stress - (22). The other curves shown are the calculated bulk wave velocity and longitudinal velocities derived from the bulk assuming a constant shear modulus ($\mu = \mu_0$) or a constant Poisson ratio ($\nu/B = \text{const.}$). Evidently the data show that the shear modulus is increasing faster with compression than the bulk modulus for aluminum. This point is consistent with ultrasonic data at low compressions - (23).

From the change in U_p between t_3 and t_{10} , ΔU_p , we can calculate the change in shear stress accompanying this quasi-elastic part of the release wave. This calculation is virtually the same as that reported by Averbach for use with velocity interferometers - (9). If we know the shear stress in the Hugoniot state, then the shear stress change upon release is a measure of the critical flow stress, or yield strength, of the compressed material. Since we now believe that the Hugoniot stress includes a shear component which may

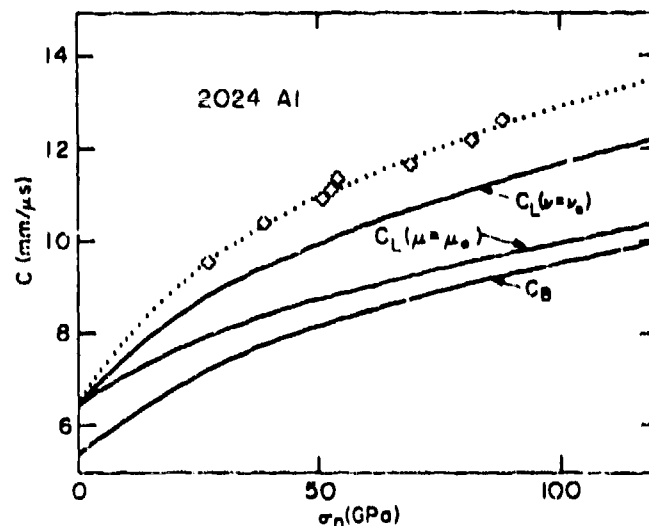


Fig. 10. Longitudinal elastic wave velocity in aluminum as a function of pressure. Other curves are the bulk wave velocity (C_B), and the longitudinal elastic wave velocity calculated using constant shear modulus and constant Poisson ratio.

be dependent on compression and temperature, extracting a yield strength from a shock experiment may be uncertain to within a factor of two. Further experiments using interferometry and ASM probes should allow us to unravel these complex phenomena.

23. "Single Crystal Elastic Constants and Calculated Aggregate Properties: A Handbook," G. Simmons and H. Wang eds., MIT Press, Cambridge, MA (1971).

SUMMARY

We have shown three new techniques developed to increase our knowledge about the high pressure-high temperature behavior of materials behind strong shock waves. These have proven to give new information about the thermal and mechanical behavior of compressed materials. The pyrometry and elastic wave measurements also provide very sensitive indicators of both solid-solid and melting phase changes which cannot be detected by conventional shock techniques. With these new means, we should be able to answer many more important questions about the properties of materials at pressures greater than a megabar.

ACKNOWLEDGMENTS

The author wishes to thank R. G. McQueen, J. N. Fritz, J. M. Brown, and C. E. Morris for many conversations and for sharing as yet unpublished ideas and data.

REFERENCES

1. J. N. Johnson and L. M. Barker, *J. Appl. Phys.* 40, 4321 (1969).
2. A. L. Ruoff, *J. Appl. Phys.* 51, 6221 (1980).
3. Q. Johnson, A. Mitchell, and L. Evans, *Nature*, 231, 310 (1971).
4. H. K. Mao, P. M. Bell, J. W. Shaner, and D. J. Steinberg, *J. Appl. Phys.* 49, 3276 (1978).
5. J. M. Brown, "Thermodynamic Properties for Iron at Very High Pressures: Implications for the Earth's Core," PhD Thesis, Univ. of Minnesota (1980).
6. D. C. Pack, W. M. Evans, and R. J. James, *Proc. Phys. Soc.* 60, 1 (1948).
7. C. E. Morris and J. N. Fritz, *J. Appl. Phys.* 51, 1244 (1980).
8. L. V. Al'tshuler, M. I. Brazhnik and G. S. Telegin, *J. Appl. Mech. Tech. Phys.* 12, 921 (1971).
9. J. R. Asay and L. C. Chhabildas in "Shock Waves and High-Strain-Rate Phenomena in Metals," M. A. Meyers and L. E. Murr, eds., Plenum, NY 1981.
10. D. E. Grady, *J. Geophys. Res.* 85, 914 (1980).
11. S. B. Kormer, M. V. Sinitayn, G. A. Kirillov, and V. D. Ustin, *Soviet Physics JETP* 21, 689 (1965).
12. R. G. McQueen, J. N. Fritz, and J. W. Hopson, *EOS* 60, 952 (1979).
13. G. A. Lyzenga and T. J. Ahrens, *Geophys. Res. Lett.* 7, 141 (1980).
14. G. A. Lyzenga and T. J. Ahrens, *Rev. Sci. Instr.* 50, 1421 (1979).
15. R. G. McQueen, J. W. Hopson, and J. N. Fritz to be published in *Rev. Sci. Instr.*
16. J. R. Asay, *J. Appl. Phys.* 46, 4797 (1975).
17. J. R. Asay, *J. Appl. Phys.* 48, 2832 (1977).
18. J. M. Brown and R. G. McQueen, *Geophys. Res. Lett.* 7, 533 (1980).
19. E. A. Kraut and G. C. Kennedy, *Phys. Rev.* 151, 668 (1966).
20. J. N. Fritz, R. S. Gaird, and R. G. McQueen, "The Use of a Magnetic Field to Measure Particle Velocity," LA-4545 MS (1970).
21. J. N. Fritz and J. A. Morgan, *Rev. Sci. Instr.* 44, 215 (1973).
22. C. E. Morris, J. N. Fritz and B. L. Holian, to be published.